AD 408 416

63-4-2

DASA-1364
URS 160-12

A FURTHER STUDY OF STRESS-WAVE TRANSMISSION

Final Report

February 1963

Prepared for
DEFENSE ATOMIC SUPPORT AGENCY
Washington 25, D.C.
Contract DA 49-146-XZ-034
Task 13.178

UNITED RESEARCH

CAMBRIDGE, MASSACHUSETTS
BURLINGAME, CALIFORNIA
BEVERLY HILLS, CALIFORNIA
CINCINNATI, OHIO
NEW YORK, NEW YORK
SIERRA VISTA, ARIZONA
WASHINGTON, D. C.

$6.60

(4) $6.60
(5) 1963 #.0

(19) Rept no.
URS 160-12

(6) A FURTHER STUDY OF STRESS-WAVE TRANSMISSION

(9) Final Report,

(7-8) NA

(11) February 1963,

(12) 70.

(13) N/A

(10)

by

H. G. Mason, V. W. Davis and J. V. Zaccor,
(5) UNITED RESEARCH SERVICES
Formerly Broadview Research Corporation
1811 Trousdale Drive
(5) Burlingame, California

Prepared for

DEFENSE ATOMIC SUPPORT AGENCY
Washington 25, D.C.
(15) Contract DA 49-146-XZ-034
(17) Task 13.178

(16) 416) NH

(18) DASA

(20) 2

(19) 13 6X

(21) N/A

ABSTRACT

This report describes the progress to date on a program to study the influence of basic soil parameters on a stress wave as it propagates through the soil. The development of equipment and instrumentation and the establishment of confidence levels in ~~such~~ equipment and instrumentation for conducting stress-wave propagation studies are discussed.

The design of a free-field soil stress gauge suitable for the stress-wave propagation studies and the evaluation tests performed to establish a confidence level for the gauge are reported.

A description is also included of the sample containment system in which the confining pressure is generated by the lateral stress and strain in the soil. This system approaches the completely confined condition with a minimum of side-wall friction effect.

Results from preliminary stress-wave propagation tests employing a controlled stress pulse of a shape that can be used to identify changes taking place in the soil as a result of the characteristics of the soil are delineated.

TABLE OF CONTENTS

LIST OF FIGURES

List of Figures (Cont'd)

List of Figures (Cont'd)

List of Figures (Cont'd)

LIST OF TABLES

Section I

INTRODUCTION

During the period from February 1960 through February 1963, United Research Services (URS) developed and established confidence levels for the necessary equipment and instrumentation to conduct stress-wave propagation studies. This work was done for the Defense Atomic Support Agency (DASA) under contract DA 49-146-XZ-034 to determine the influence of basic soil parameters on the stress wave as it propagates through the soil. A description of development work and the results of stress-wave propagation tests are in this report; early work was described in greater detail in Reference 1.

The long-range objective of this work is to study the transmission of plane stress waves in soil materials, particularly the energy loss and distortion of the stress pulse during propagation as a function of basic soil parameters such as air pore pressure, compressibility, grain size, moisture content, relative density, void ratio, shear strength, lateral strain, and axial stress level. The fundamental goal of this study is to understand the basic mechanisms of soil behavior caused by a propagating stress wave so that theories can be developed that take into consideration the importance of each soil and loading parameter for practical applications.

In the first phase of this program, the over-all stress-wave propagation problem was analyzed to aid in the selection of the general experimental approach and a suitable experimental methodology for applying the load, for sample containment, and for measuring the desired parameters. Although it is difficult to produce experimentally, a plane-wave test geometry was considered best because it has the advantage of providing known side boundary conditions amenable to theoretical analysis. A cylindrical sample surrounded by a totally contained fluid boundary layer, loaded axially with a plane wave was considered the most desirable configuration because of the encouraging results obtained with

it in reducing side-wall friction and providing the lateral support necessary to simulate the plane-wave geometry. (The system is described in References 1 and 2.)

During the first phase of the program, the minimum measuring requirements were considered to be gauges for measuring characteristics of the stress waves generated at the loading end of the sample and characteristics of the stress waves (including air pore pressure) after passage through all or a portion of the sample. Since it was deemed important to make such measurements at several locations within the length of the sample, free-field stress gauge development became an important part of this work.

Work completed during the contract period on DASA contract DA 49-146-XZ-019, also being conducted at URS, showed the fluid confinement of the sample to have additional advantages, in that a sample average lateral, soil stress measurement is possible by monitoring the fluid pressure as a function of time.

During the period from October 1961 through February 1963, effort was focussed on further gauge and equipment development, on establishment of confidence levels for the equipment and instrumentation, and on stress-wave propagation studies. The former two constituted the major portion of the effort. Since the specific objective was to investigate behavior of a stress wave as influenced by individual soil and loading parameters, it was necessary to develop an input load of such a nature that the influence of soil and loading parameters on the stress pulse shape could easily be observed and interpreted. Next, it was necessary to obtain stress-time histories at several points within the sample to observe any changes that might occur as a result of the stress wave passing through a known length of soil. To be able to interpret these stress readings, however, it was necessary to establish a confidence level, i.e. it was necessary to know what experimental error to expect. And last, by making actual stress-wave propagation observations, it was possible to establish how the actual experimental equipment could best be constructed.

This work was done by the Soils and Structural Mechanics Group of United Research Services under the administration of A. B. Willoughby, General Manager, Burlingame Research Center. H. G. Mason, Project Manager, was supported by Messrs. C. K. Wiehle, V. W. Davis, and J. V. Zaccor. The cooperation and technical support of Lt. Comdr. J. J. Healy, Maj. Patrick J. Donohoe, and John G. Lewis, DASA project officers, is gratefully acknowledged.

Section II

EQUIPMENT DEVELOPMENT

FREE-FIELD STRESS GAUGE

Since a free-field stress gauge is in reality a small structure, its design must recognize soil-structure interactions so that the gauge can read free-field stresses accurately. Other considerations in the basic design must include such parameters as the sensitivity of the sensing unit to stresses from other directions than those of interest and to the effects of nonuniform loading. The gauge configuration described in Reference 1 embodied these concepts.

It was anticipated that arching effects around the gauge and nonuniform stress distribution on the gauge surface would be two of the major difficulties in obtaining free-field stress readings.

Arching effects occur if the compressibilities of gauge and sample material differ and if the sample material possesses some shear strength. As a result of arching, the stress on the gauge surface differs from that in the sample material when the gauge is not present. If the gauge is less compressible, more rigid than the sample, as in the present application, the stress on the gauge is greater than the free-field stress; if the gauge is more compressible, less rigid, the stress on the gauge is less than free-field stress. These effects are called passive and active arching, respectively. The difference in stress on the gauge owing to arching effects increases with increasing shear strength. In the case of passive arching (gauge less compressible than the medium), the greater the shear strength of the medium the more it is able to transfer the axial load to the gauge from a region in the sample not directly above the gauge. Since arching effects are dependent upon both compressibility and shear strength of the material, it is possible to have high compressibility and still have little arching effect if the material has low shear strength.

If the medium were elastic, the arching stress on the gauge in the present application could be estimated from the following approximate relationship from Reference 3:

$$P_a \simeq \frac{\pi E}{2D}[z] = \frac{\pi E}{2D}[\frac{1}{2}\Delta]$$

where P_a = arching stress, the difference between free-field stress and stress on the gauge

E = modulus of elasticity of the medium

D = diameter of the gauge

z = relative displacement between one end of the gauge and the medium

Δ = change in length of a section of medium under free-field stress whose initial length is equal to the thickness of the gauge

Since the medium is assumed elastic and the gauge, rigid; Δ is given by:

$$\Delta = \frac{PL}{E}$$

where P is the free-field stress and L, the thickness of the gauge.

Combining these equations gives

$$\frac{P_a}{P} = \frac{\pi}{4}\frac{L}{D}$$

The ratio of arching stress to free-field stress is seen to be proportional to the thickness to diameter ratio. For this reason, a wafer type gauge configuration was used.1/

1/ Effects on this ratio are discussed further in Section III.

The first piezoelectric type free-field stress gauge which gave readings in an acceptable range in materials exhibiting low shear strength is shown in Figure 1. It is wafer-shaped, approximately 3/4 inch in diameter and 0.030 inch thick, and is placed in the sample with its plane perpendicular to the direction of stress. Because the piezoelectric wafers are sensitive to edge loading, it was necessary to protect the edge of the wafer from lateral stress by means of an annulus of stiff material. The stiff annulus is separated from the wafer by a 0.015-inch air space. Steel shim plates placed on each side of the wafer isolate the edge of the piezoelectric wafer from air load and also serve as solder terminals for the lead wires. Adhesive is used for all bonds within the wafer. Silver paint and adhesive on the piezoelectric wafer surface ensure tight electrical contact between the wafer and terminal plates.

Since piezoelectric gauges are charge producing devices, there is always some difficulty in maintaining a good low frequency response with such gauges. A high input impedance preamplifier must be used, and special care is required to ensure no low resistance leakage paths to ground. The reflected stress gauge, for example, can adequately measure for at least 300 milliseconds if such precautions have been taken. These special precautions have not yet been taken with the free-field stress gauges since primary interest has been with the more fundamental problems such as the effects of arching and bending. Thus, some of the data obtained to date with these gauges show some signal decay owing to charge leakage. No difficulty has been experienced, however, in holding these gauges up for the 20 or 30 milliseconds required in the transmission study.

Additional effort was expended during the latter part of the contract to develop a gauge that also reads with an adequate response in soils exhibiting appreciable amounts of shear strength. Each gauge component was investigated to determine how it influenced the accuracy of the gauge when compared with air calibration. Approximately 30 different gauges were fabricated to test various principles and methods of fabrication. This effort resulted in the design illustrated in Figure 2. The gauge consists of a 1/4-inch diameter piezo-

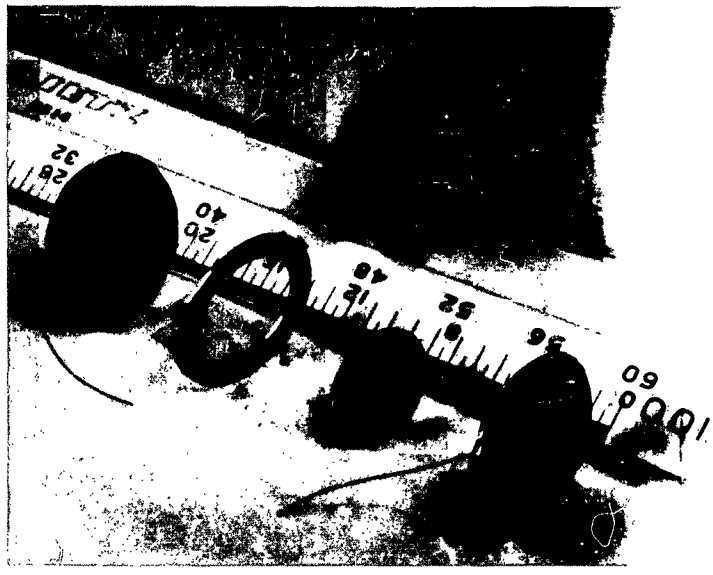

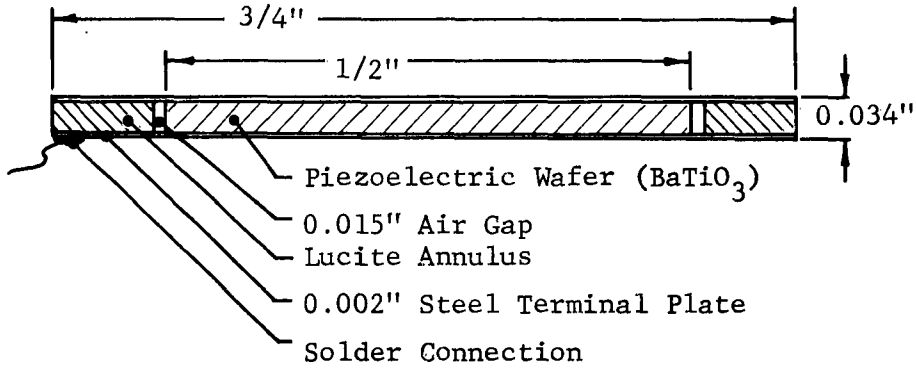

Figure 1

INITIAL FREE-FIELD STRESS GAUGE
DESIGN, TYPE I

electric wafer, 0.010-inch thick, mounted between two conducting pedestals and surrounded by a segmented annulus. The top and bottom of this assemblage are covered with conducting terminal plates. Conducting paints, glues, and insulating gaskets are used in the gauge to provide the connections, bonds, and insulations necessary for proper electrical operation and sealing of the gauge configuration against air leaks.

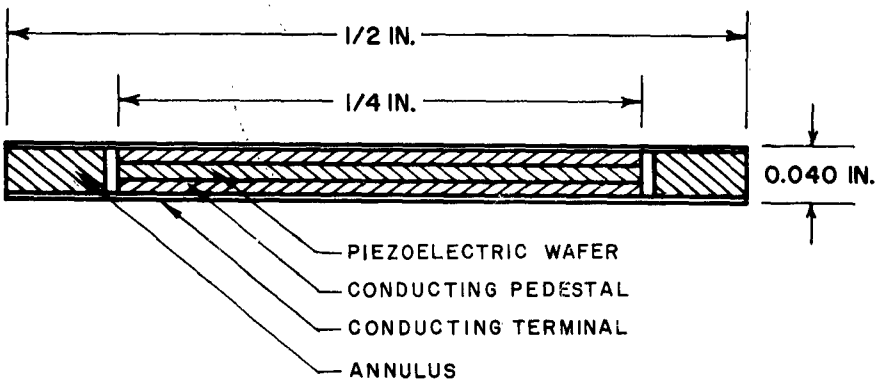

Figure 2

PRESENT FREE-FIELD STRESS GAUGE DESIGN, TYPE II

AIR PORE PRESSURE GAUGE

To determine the effect of interstitial air on stress-wave propagation it was necessary to develop an air pore pressure gauge that was capable of isolating the air pressure from the intergranular stresses and still not restrict the response of the gauge to any appreciable degree.

Such an air pore pressure gauge was developed for use in the gauge response and stress-wave transmission studies.

The gauge is illustrated in Figure 3. It consists primarily of a hollow, piezoelectric ceramic cylinder placed in a well in a lucite cup and covered by a porous stone. The completed gauge is 3/8 inch long and 1/4 inch in diameter. The piezoelectric cylinder is 1/16 inch in diameter and has a 0.015-inch wall thickness. It is glued in place at the base of the well in the cup with a flexible bond of rubber cement. This was found to better isolate the cylinder from cup distortion resulting from intergranular stress. The top of the cylinder is covered by a 0.010-inch acetate cap. A 0.001-inch acetate diaphragm is placed over the well to isolate the cylinder walls from air load. The diaphragm is loaded by air pore pressure through a porous stone, thus loading the cylinder in a length expander mode. The electrical leads are 0.005-inch insulated wire, connected to the cylinder with silver paint. The wire is led through the cup wall and cemented to hold the wire in place in the wall and to form an air seal.

EXPERIMENTAL TEST APPARATUS

Although most of the basic features of the test apparatus described in Reference 1 have been maintained, the equipment has been improved considerably. The apparatuses shown in Figures 4, 5, 6, and 7 have three main elements: the loader, the sample container, and the measuring system.

The loading system varies with the type of load required. To produce a step wave of infinite duration, the modified shock tube described in Reference 1 is used; to produce a square wave pulse, a classical shock tube loader of the proper proportions is used.

The sample container is a heavy-walled steel cylinder, large enough to hold soil samples 1-1/2 inches in diameter and up to 1 foot in length. As illustrated in Figure 7, the soil sample is contained on the sides by a closed fluid system within the steel cylinder. This fluid side boundary

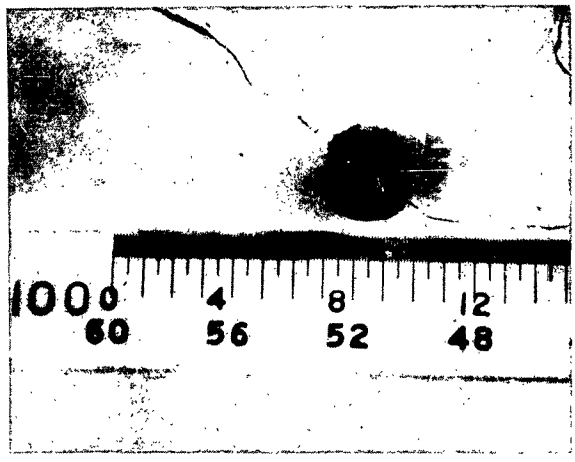

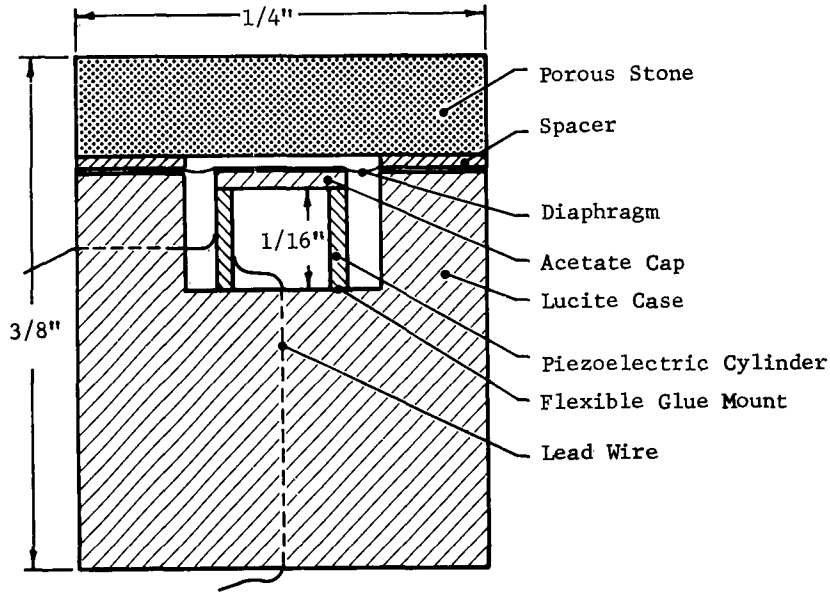

Figure 3

AIR PORE PRESSURE GAUGE

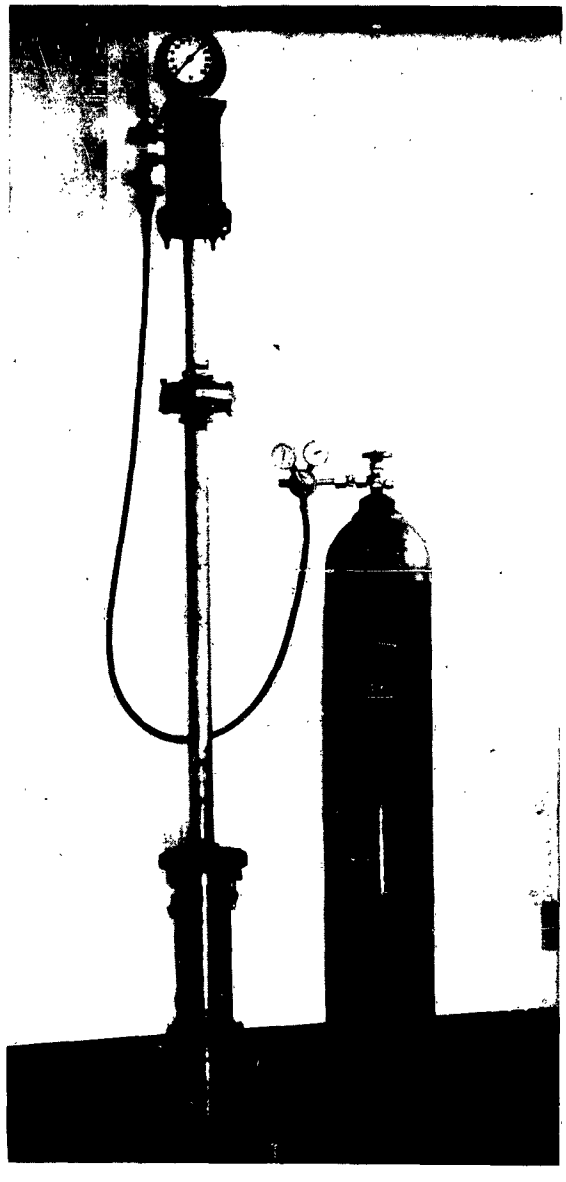

Figure 4

TESTING APPARATUS, SQUARE WAVE PULSE CONFIGURATION

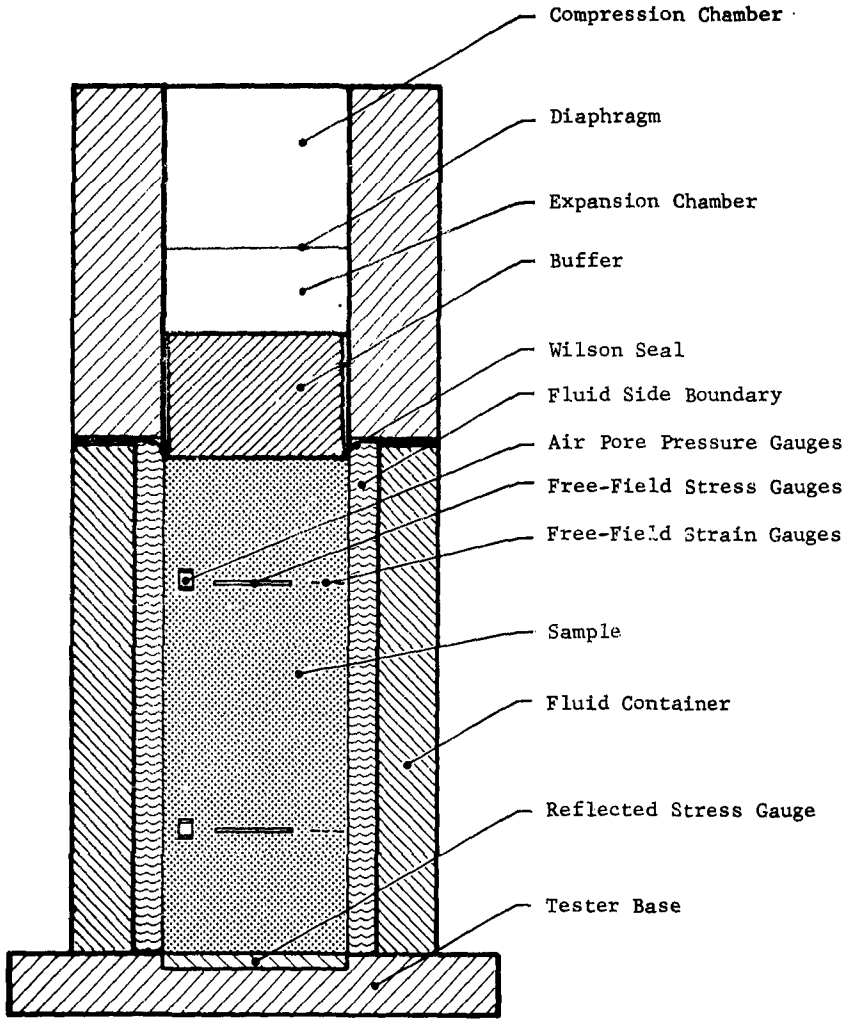

Figure 5

CONCEPTUAL SCHEMATIC OF THE SOIL TESTER, BUFFER LOADED SAMPLE

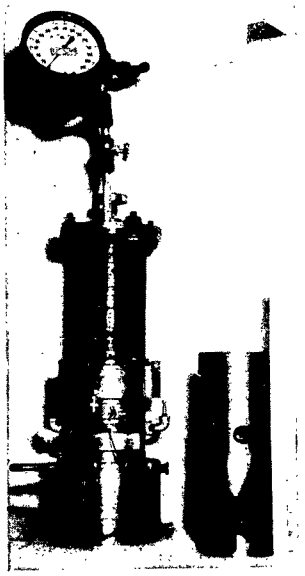

Figure 6

TESTING APPARATUS, STEP WAVE PULSE CONFIGURATION

Note: The soil tester which is on the left is set up for a 1-1/2 inch long sample. A 1-foot long sample container is on the right.

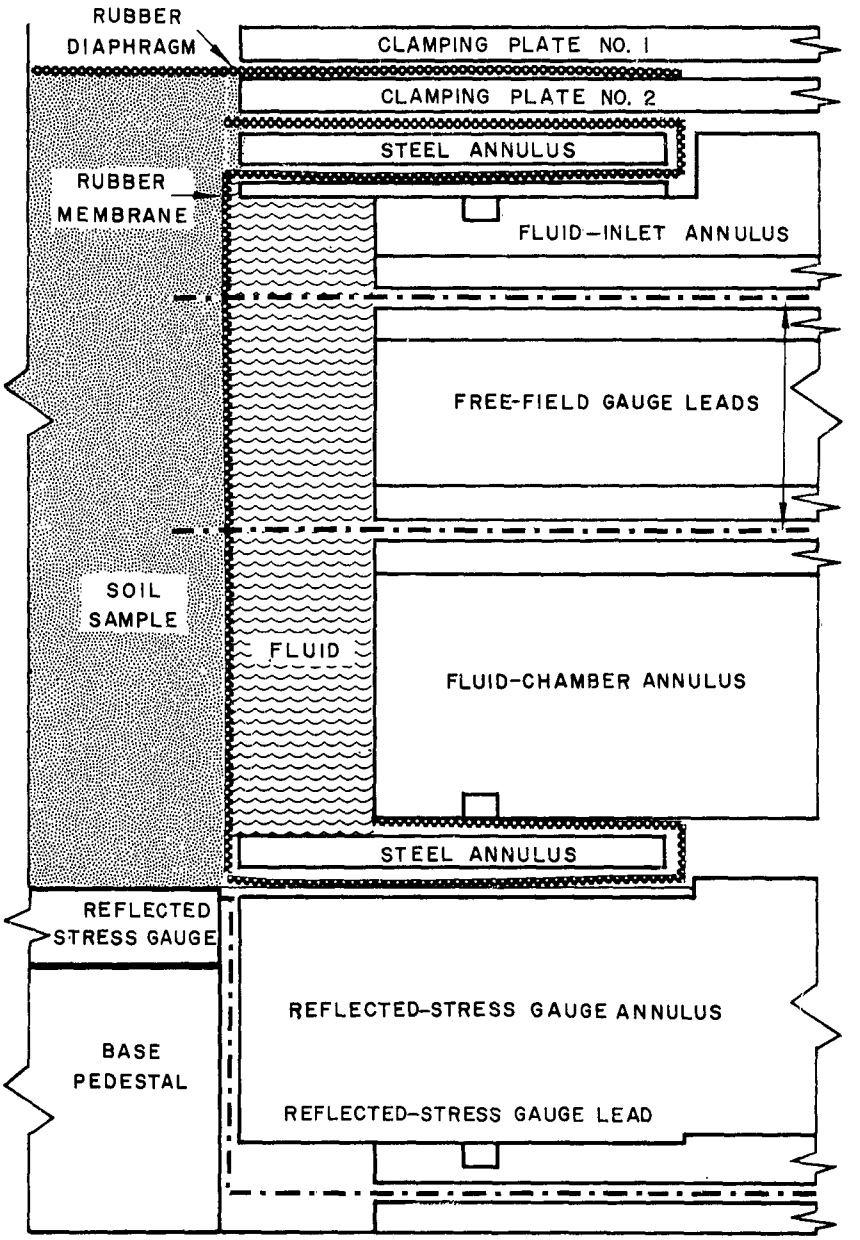

Figure 7

SCHEMATIC OF THE FLUID BOUNDARY

Note: Rubber diaphragm at loading end of sample

allows control of average lateral strain with a minimum of side-wall friction and allows simulation of a number of boundary conditions. A 0.010-inch thick rubber membrane separates the fluid and the sample. The membrane is fastened to the steel container at both the top and the bottom.

In tests where the maximum surface displacements are less than 3/8 of an inch, the sample is placed within the boundary and brought up through a 3/8-inch thick steel ring at the top of the loader to prevent direct loading of the fluid boundary by the air load.[1/] A thin rubber diaphragm (dental dam) prevents the air shock from penetrating the voids in the soil, while permitting the entire load to be applied to the sample.

In tests where the maximum amount of displacement of the surface of the sample is greater than 3/8 of an inch, the tester is operated with a buffer, similar to that described in Reference 2, to avoid the possibility of loading the fluid boundary.

To assemble the sample container, the rubber membrane is retained at the bottom end of the sample by means of a 0.050-inch thick steel annulus. A 0.005-inch thick acetate annulus is placed next; the steel fluid chamber annulus with a 2.00-inch inside diameter is centered over it. The lead wires, 0.005-inch single conductor enamel insulated wire, which have been previously threaded through the rubber membrane wall and sealed against leaks, are soldered to plugs in the steel boundary walls. An acetate annulus identical to the one on the bottom is centered over the steel fluid-chamber annulus. Above this is placed another portion of the steel fluid-chamber annulus, specially machined to provide inlet and outlet

1/ This arrangement develops a small amount of side-wall friction which can be significantly reduced by recent improvements that can be used in future work.

channels for filling the boundary without trapping air in the system. The upper end of the membrane is stretched over a steel annulus which fits into a slight aligning recess at the top of the fluid chamber. The membrane is held in place by folding it back over a thin metal annulus which is clamped in place by bolting a clamping ring to the base to hold the fluid boundary together. The resultant boundary, which is 1/4 inch thick, is then filled with silicone oil and sealed.

Silicone oil was selected for use in the fluid boundary because it is a good insulator which helps maintain good electrical response of the free-field gauges. It has low viscosity to help satisfy the condition of low side-wall friction on the sample, and does not react with or weaken the rubber membrane, all of which are requirements of the fluid in the boundary.

A Kistler Instrument Corporation 605 pressure transducer was placed in the steel fluid-chamber wall to obtain lateral stress by measurement of fluid pressure. The transducer was selected because of its small size and its low displacement under load.

In preparation for a test, the soil container is filled with soil to the level at which free-field and air pore pressure gauges are to be placed. A gauge is then soldered to the leads, which were threaded through the wall of the rubber membrane, and the gauge is seated in the soil. The leads are carefully placed to avoid "cross talk" between gauges and false signals resulting from the gauge wires.[1/] Additional soil is carefully placed over the gauge until the level of the next gauge is reached. This procedure is continued until the top of the soil container is reached. The sample is screeded, and the rubber diaphragm

---

1/ When the two leads to a gauge are close to each other, small changes in the distance between them will result in capacitance changes that give a false signal.

is placed over the soil. The loader is clamped over the diaphragm to the soil container so that the diaphragm forms a seal between the air load and the soil sample.

The stress at the lower end of the sample is measured by means of the reflected-stress gauge, a 1-1/2 inch diameter piezoelectric ceramic wafer bonded to the 4-inch thick steel base to ensure a rigid end boundary of uniform characteristics over the entire end of the sample. Such uniform characteristics avoid the problems of stress distortion in the vicinity of the gauge due to differential motion of the gauge with respect to the remainder of the boundary. By careful control of leakage paths and by the use of a high input impedance preamplifier, the low frequency response of the reflected-stress gauge is good enough so that stresses can be monitored for times as long as 300 milliseconds.

An air pressure gauge mounted in a steel annulus, located immediately upstream from the air-soil boundary, monitors the input air loading. It consists of a 1/8-inch diameter piezoelectric ceramic cylinder mounted so that it is loaded axially. A more detailed description of the gauge is given in Reference 4.

To operate the tester to produce a step wave of infinite duration, the compression chamber is pressurized to the desired level, and the diaphragm between the compression and expansion chambers is punctured by means of a plunger rod. The resultant shock wave loads the sample through the buffer or rubber diaphragm located at the upper end of the sample. The shape of the wave is controlled by a system of screens and baffles in the compression and expansion chambers.

To operate the tester to produce a pulse approximating a square wave, a classical shock tube is used which has the proper relation between the length of the expansion and compression chambers to give the desired shape and duration. In this operation the compression chamber is pressurized to the desired level, and the diaphragm between the compression and expansion chambers is either punctured mechanically or

by means of employing a diaphragm of predetermined strength, which will burst at approximately the desired pressure. The resulting shock wave loads the sample through the buffer or rubber diaphragm. Additonal wave shape control can be provided by a system of screens and baffles in the compression and expansion chambers.

DYNAMIC FREE-FIELD SOIL DISPLACEMENT MEASURING SYSTEM

Feasibility Study

The initial effort to devise a dynamic free-field displacement detecting device for use with the soil column began with a study of the potential of a very sensitive dynamic capacitance detecting system. A system with adequate response characteristics was available at URS so that only the development of a suitable probe was required. The extraneous parallel capacitances arising from the body of the tester and other portions of the equipment made it apparent quite early that a sufficiently sensitive probe for continuous reading would not be compatible with the design of the apparatus. Consequently, another type of probe for discrete step sensing was considered. It consisted of laminated layers of conducting and dielectric material. Alternating 0.001-inch layers were tried in an experimental arrangement to determine probe to ground spacing requirements. The system was found inadequate because of the close proximity requirement. Expected lateral displacements under load would exceed the necessary spacing, and the lateral soil boundary would be driven into the probe.

A commercially available optical tracking device was considered next. This instrument projects a beam of light which, if partially refelcted and partially absorbed or scattered by a suitable target, will follow displacements of 0.100 to 2.000 inches (depending on lens used) with a resolution of 0.01 per cent and tracking speeds up to 100,000 ft/sec. Requirements on the test apparatus were limited to an optical path to the soil column and a suit-

able target that would follow the axial motion of the soil. The device capability was demonstrated, and an actual free-field displacement-time measurement for a point on the column was made.

Experimental Tests

The optical tracking equipment appears to offer the greatest expectancy of providing the difficult, though necessary, measurements. Three different types of targets were prepared for testing. To provide an optical path, three free-field stress gauge lead ports were removed, and lucite ports were installed. Because the opacity of the present membrane at the fluid-soil boundary precluded locating the target in the soil, the targets were affixed to the membrane opposite the optical entries.[1/] The targets consisted of (1) a white line painted on the membrane, (2) a horizontally mounted length of 0.008-inch diameter wire glued to the membrane, and (3) a 0.001-inch thick sheet of 1/8-inch square stainless steel shim stock with the lower half painted black, also glued to the membrane. The third target was the only one that could be "locked onto" for tracking with the optical paths obtained. It was the opinion of the demonstrating engineer that a slightly more transparent optical path would have made the second target also suitable.

When the tracking device was "locked on" the third target, a pulsed load was applied. In mounting the target, however, it was placed too low in the optical path, and the total deflection under load was too great to keep the target lined up with the optical port. A subsequent pulsed load at a lower pressure was applied, and the target remained within the optical path so that an excellent displacement-time trace was obtained.

A comparison of the results was made with data available from contract DA 49-146-XZ-019. The data appeared to be in agreement within the experimental limits of error.

1/ Additional tests, however, indicated that for the translucent membranes used in contract DA 49-146-XZ-019, a target affixed to the buffer inside the membrane could be tracked. It would, therefore, be possible to track targets located in the edge of the free-field soil column.

Section III

EQUIPMENT EVALUATION

FREE-FIELD STRESS GAUGE

A number of tests were conducted under various conditions to establish a confidence level for the equipment and instrumentation. Once a confidence level has been established, it is possible to acquire useful data. As new problems arise and understanding increases, subsequent re-evaluation of the equipment and instrumentation is required to determine the effect on the confidence level so that the data may be made more meaningful.

The performance of a free-field stress gauge is difficult to evaluate since the exact stress conditions in any given soil sample are unknown. However, by evaluating it under a number of conditions, it is possible to establish a confidence level with which to work.

Free-field stress gauges of the Type I design shown in Figure 1 were evaluated in various sample materials in the URS testing apparatus shown in Figure 6. The tests were conducted for loading pressures ranging from 30 to 70 psi with rise time to equilibrium stress ranging from 1 to 10 milliseconds.

Measurements of the equilibrium stress were made with the reflected-stress gauge at the end of the samples. The reflected-stress gauge readings at equilibrium were taken as true sample stress because the gauge is free of bending effects due to its rigid mount and is not subject to arching effects since it has the same diameter as the sample. Tests of this nature have furnished response data for the free-field stress gauges in air, in glass-bead mica-flake

samples of several compressibilities, and in Ottawa sand samples.

A typical record of voltage output versus time for the free-field and reflected-stress gauges in a glass-bead mica-flake material is shown in Figure 8. In this particular test, the material consisted by weight of 80 per cent glass beads and 20 per cent mica flakes (80/20), with a range of particle sizes from 9,700 to 19,500 microns for both materials. The sample was 1-1/2 inches long with the free-field stress gauge mounted in the center of the sample. The gradual decay of the trace for the free-field gauge is attributed to charge leakage.

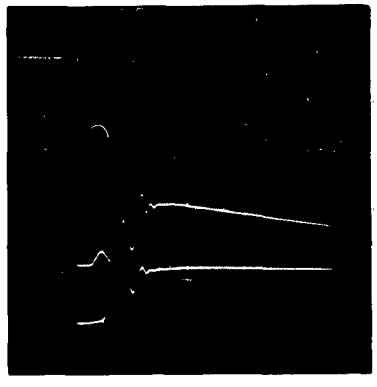

Figure 8

OUTPUT VOLTAGE VERSUS TIME FOR THE FREE-FIELD AND REFLECTED-STRESS GAUGES

Note:
Upper trace: 500 mv/division
(free-field) 2 msec/division
Lower trace: 10 v/division
(reflected 2 msec/division

The output of the gauge at three equilibrium stress levels in a 80/20 sample material is compared with the air calibration in Figure 9. The average of the output voltage from four tests is within ±5 per cent of the air calibration, but the individual readings have a spread of +6 or -7 psi, most of which can probably be attributed to sample preparation. The average gauge output from the test results shown in Figure 9 for 95/5 material agreed with the air calibration, but only when a new sample material was used for each test. If the material was simply stirred and loosened between tests, the average output was higher than

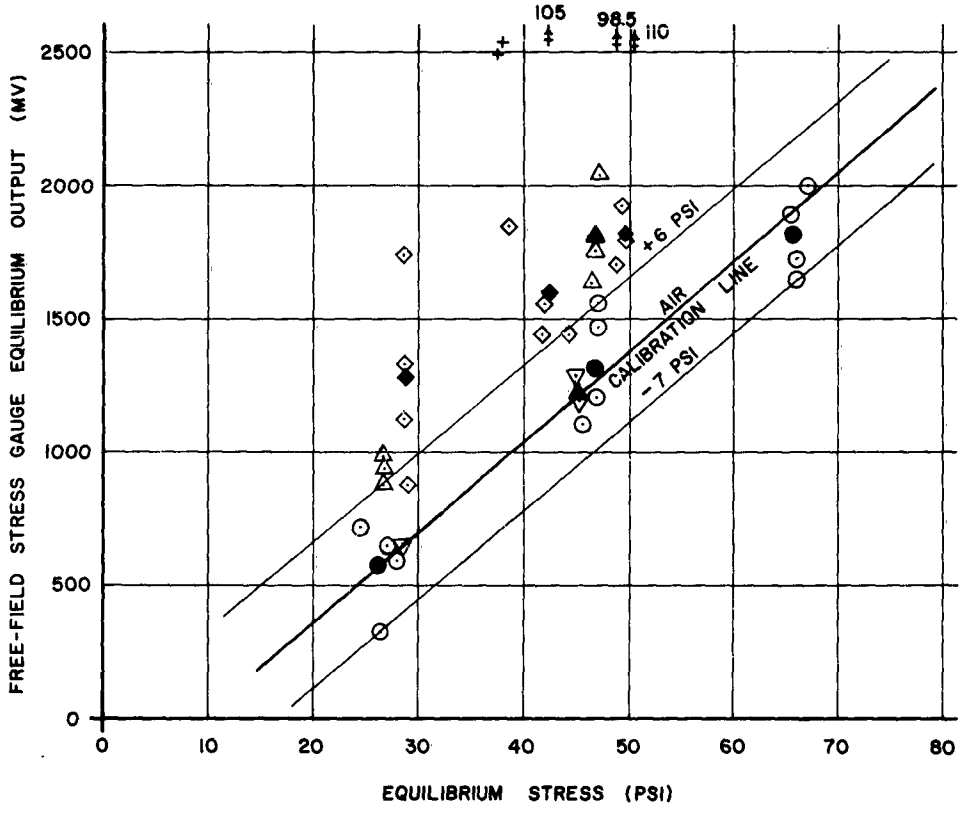

Figure 9

FREE-FIELD STRESS GAUGE TYPE I OUTPUT VERSUS FREE-FIELD STRESS

Note:
- ⊙ 80/20 samples
- ● 80/20 average
- △ 95/5 stirred sample
- ▲ 95/5 stirred average
- ▽ 95/5 fresh sample
- ▼ 95/5 fresh average
- ◇ 100/0 sample
- ◆ 100/0 average
- \+ Ottawa sand sample
- ↟ higher than graph
- 110 equivalent to 110 psi

the air calibration, about 25 per cent at 50 psi. Results for tests using 100 per cent glass-bead material averaged 30 per cent higher than the air calibration at 50 psi, as shown in Figure 9.

Test results indicate that excess gauge output in the mixed materials might be associated with the percentage of the glass-bead component. This result would be expected if the glass beads exhibit greater shear strength than the mica flakes, since greater shear strength would result in greater arching stress on the gauge.

As indicated in the tests on a 95/5 material, the spread in the readings could reflect the method of preparing the sample for a test. The method for much of the work consisted of stirring and loosening the two components between tests which could have resulted in variations in sample component distribution. Results of static compression tests have indicated how sensitive the compressibility of this material is to the proportions of the two components present. For instance, under a 100-psi load, the compressibility varies from 10 to 65 per cent when the ratio of comnents is varied from 100/0 to 80/20, respectively. The variations in shear strength and compressibility result in nonuniform loading of the gauge and variations in magnitude of arching effect.

When the Type I gauge design was used in an Ottawa sand sample, the average gauge output voltages from the test results were more than 100 per cent higher than in the glass-bead mica-flake mixtures, shown in Figure 9. Because of this large overregistration, additional gauge development was begun, which resulted in the Type II gauge design shown in Figure 2.

With increase in accuracy of the new design, it became evident that the actual diameter of the sample had an important effect on the gauge evaluation.[1/] In attempting to eliminate this effect from the evaluation, several approaches were considered. The best approach seemed to be to place the gauge near the surface of a large sample.

1/ This effect is discussed in greater detail in the discussion of the soil loader and sample container.

Since the URS gauge measures only dynamic stresses, it was necessary to conduct the evaluation tests in a dynamic loader. The largest dynamic loading device available was the URS 4-inch square shock tube. In these tests, the gauge was located in the middle of the sample 1/4 inch below the surface, close enough to the surface to ensure little stress loss from side-wall friction. The sample was loaded through a rubber diaphragm by a 50-psi flat-topped air shock, 10 milliseconds in duration. The soil sample was 20-30 Ottawa sand placed at a density ranging from 99 to 106 pcf.

The actual stress level on the sample is the result of and equal to the pressure of the air shock reflected off the air-soil boundary. This air shock pressure is measured by means of an air pressure gauge located in the air medium near the air-soil boundary.

Based on the air input pressure of 50 psi, the average gauge readings of the best designed gauge 1/ ranged from 4.5 to 7.5 per cent low, with spreads ranging from ±4 per cent to ±12 per cent. Typical test data are presented in Figure 10. However, based on a stress of 45 psi for the 1/4-inch depth, which was arrived at by plotting the stress readings with depth and extrapolating back to the surface, the average gauge readings were 3 to 7 per cent high.

As discussed in Section II if a gauge is less compressible than the soil, passive arching occurs; however, by making the gauge wafer-shaped, it was hoped to minimize the magnitude of the effect. It was also recognized that

---

1/ Small variations in gauge design and fabrication techniques had pronounced effects on gauge response. For instance, changes in type of bonding materials resulted in gauge readings that were 20 to 40 per cent in error, see Figure 10.

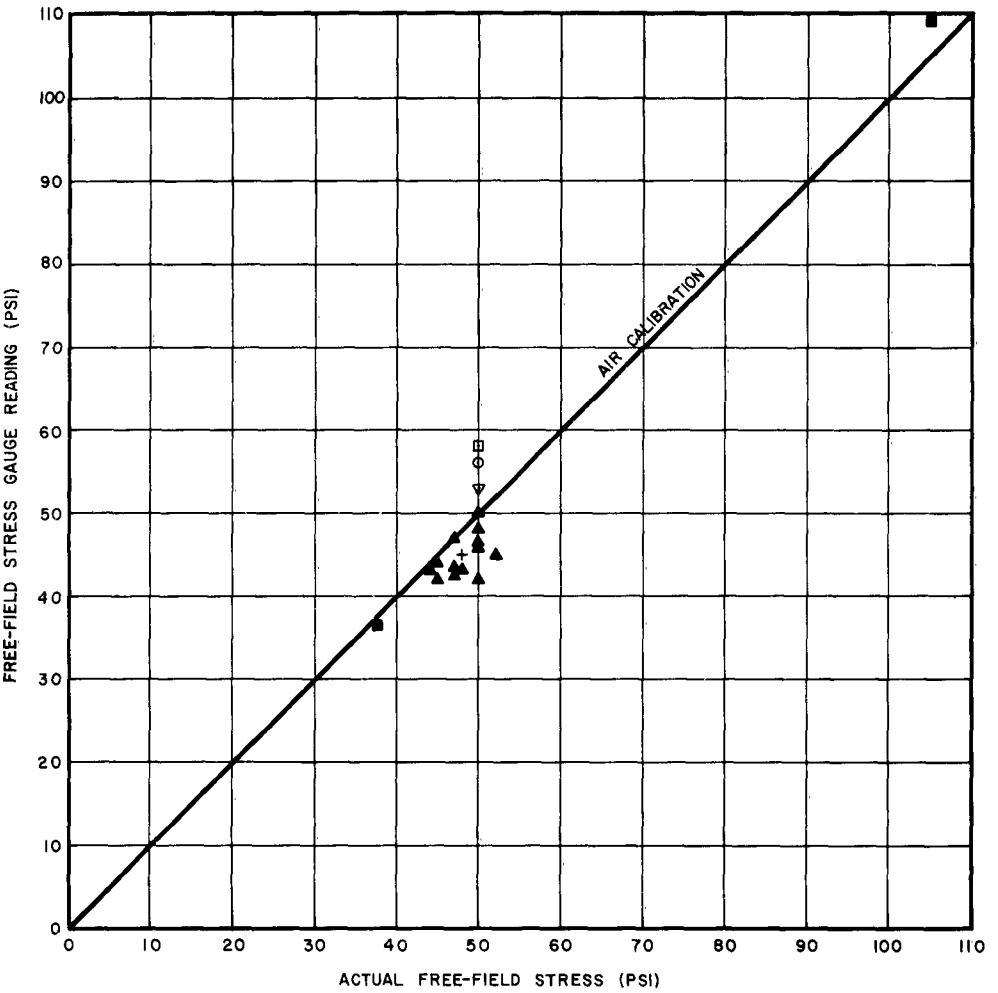

Figure 10

TYPICAL FREE-FIELD STRESS GAUGE RESPONSE

Notes: Each point represents one or more tests. Data include tests on two gauges of the same type in both loose and dense sand.

▲ Type IIA at 1/4-inch depth in shock tube--loose Ottawa sand
+ Type IIA average--45 to 50 psi range
⊙ Type IIB average
⊡ Types IIC and IID average
▽ Type IIE average
■ Type IIA at 1/4-inch depth in LDDL--loose Ottawa sand

sufficient cover over the gauge would be required to develop full arching. Inasmuch as the gauge is much less compressible than the soil in which it is placed, it was felt that, if arching was to be significant, the gauge would show an increase in load as the cover over the gauge increased.

Additional tests were performed with the gauge placed at various depths greater than 1/4 inch to evaluate this effect. However, a line drawn through these data points indicates a loss of the entire stress pulse due to side-wall friction by the time stress has reached a depth of three times the diameter of the sample.

Figure 11 shows this effect and illustrates the relationship of stress loss as a function of the ratio of depth to diameter of the container for three different sized containers and two different soils. This relationship is in fairly good agreement with what has been observed by other experimenters.

These tests while informative did not prove that an insignificant amount of arching existed since the effect could have been due to active arching, although it appeared inconceivable that the gauge was more compressible than the soil, and result in zero stress readings at depths three times the diameter of the soil container. Attempts were made to evaluate the results in the fluid boundary container; however, the sensitivity of the gauge readings to the actual diameter of the sample made it difficult.

Another approach was then attempted, i.e. evaluating gauges in which arching effects were sure to be much more pronounced in both the active and passive cases. Two gauges (Types III and IV) were designed to provide passive arching. Type III was essentially the free-field stress gauge design mounted on a 1/4-inch long metal rod thereby giving a diameter to length ratio of 2. The Type IV gauge was mounted on a 1-inch rod to further the increase of the passive arching effect. Another gauge (Type V) was designed to provide active arching. It was essentially the same design except it had 1/4 inch of foam rubber inserted in the 1-inch

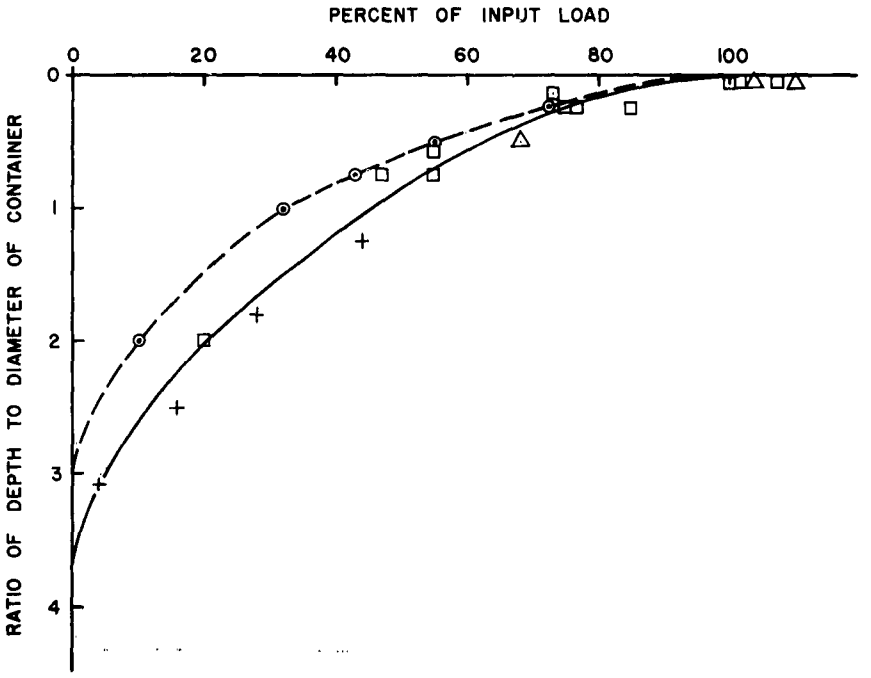

Figure 11

EFFECT OF SOIL CONTAINER SIDE-WALL FRICTION ON GAUGE READINGS

Notes: □ 4-inch square shock tube--loose 20-30 Ottawa sand
△ 12-inch diameter loader--loose graded Monterey sand
+ 19-inch diameter loader--loose 20-30 Ottawa sand
⊙ 12.0 by 13.5 foot wooden silo--wheat with = 30 deg.

length. The side walls of each gauge were covered with teflon to reduce side-wall friction on the gauge.

As shown in Figure 12 by uncorrected data, the Type III gauge readings increase with depth for a very short depth at which time the decrease in free-field stress due to side-wall friction becomes larger than the amount of over-registration due to arching and the resultant load on the gauge decreases toward zero at three times the diameter of the container. Applying a correction for stress at depth from Figure 11, we obtain the corrected curve shown in Figure 12. A similar curve is shown for gauge Type IV. The effect of the active arching, i.e. an appreciable decrease in stress for the very compressible structure, is shown by the point plotted for gauge Type V.[1/]

To determine the effect of gauge orientation, shock tube loadings were made and readings were taken with the gauge oriented at 0, 30, 45, and 60 degrees to the direction of the stress-wave propagation (90 degrees being normal gauge orientation). Using the 0 degree orientation reading as the stress in the lateral direction [2/] and the 90 degree orientation reading as the stress in the axial direction, the stress in each of the other two orientations was calculated by a simple resolution of component forces to determine the stress normal to the gauge face.

1/ Data taken in connection with work being done at URS under contract AF 29(601)-5537 for the Air Force Special Weapons Center in the URS Long Duration Dynamic Loader (LDDL) have confirmed both the side-wall friction and arching effects.

2/ These lateral stress readings agreed favorably with those obtained from fluid pressure measurements in the device shown in Figure 6.

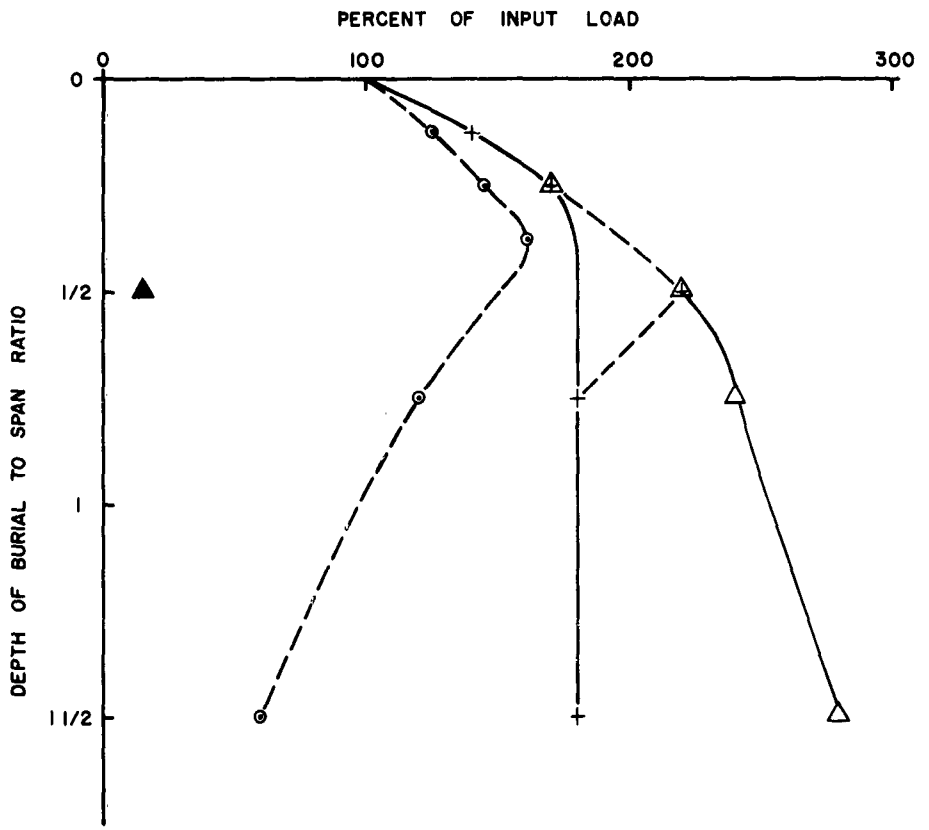

Figure 12

EFFECT OF PASSIVE AND ACTIVE ARCHING ON GAUGE RESPONSE

Notes:
- ⊙ Uncorrected data from Type III gauge with a diameter to length ratio of 2
- \+ Data corrected for side-wall friction of the container, Type III gauge with a diameter to length ratio of 2
- △ Data corrected for side-wall friction, Type IV gauge with a diameter to length ratio of 1/2
- ▲ Data corrected for side-wall friction of the container, Type V gauge with a diameter to length ratio of 1/2

The calculated value was obtained from the equation:

$$\sigma_\theta = \sigma_1 \sin^2 \theta + \sigma_3 \cos^2 \theta$$

where σ_θ = stress on gauge surface

θ = angle between gauge surface and axis of sample

σ_1 = measured axial stress

σ_3 = measured lateral stress

This comparison showed the gauge readings to be 10 per cent below the calculated value. The low readings may be attributed to arching or bending of the gauge, due to nonuniform stress distribution over the gauge, especially in the 0 degree orientation since this is the poorest configuration of diameter to length ratio for the gauge. What effect arching in this orientation has on the lateral stress is not known.

The data suggest that the gauge can be placed up to 10 degrees on either side of the 90 degree position and still read the axial stress within 5 per cent.

To determine the sensitivity of the gauge to accelerations, the gauge was isolated from sample stress by enclosing it in a steel cup. The cup was placed in the sample at a depth of 1/2 inch, and the sample was loaded in the normal way. In Figure 13, the output of the gauge for the test is compared with the normal output for a free-field stress gauge, placed at the same location under the same loading and gain settings. The maximum signal from the acceleration tests was only 6 per cent of the free-field stress signal and lasts only during the very early part of the time of interest.

The increase in stress after the initial rise which is seen in the normal gauge output records is due to the

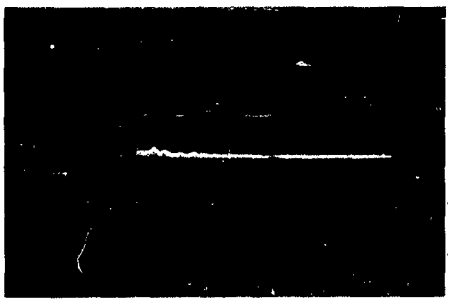

Gauge acceleration output

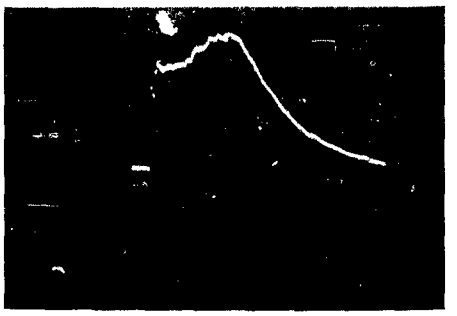

Normal gauge output

Figure 13

ACCELERATION SENSITIVITY OF FREE-FIELD GAUGE

Note: Approximate grid scale
Vertical: 10 psi/5mv/division
Horizontal: 2.8 msec/division

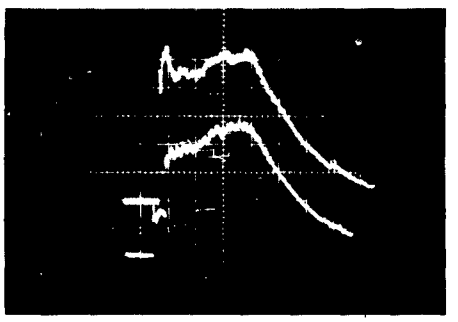

Upper trace: Typical free-field stress gauge reading--approximately 10 psi/5mv/vertical division

Lower trace: Typical air pressure gauge reading--approximately 18 psi/v/vertical division

Figure 14

TYPICAL SHOCK TUBE RECORD

contact surface in the air shock wave; it is also evident on the air pressure gauge output as shown in Figure 14.[1/]

The next step in the evaluation of the free-field stress gauge was to verify side-wall friction effects. A 1-1/2 inch long sample contained in the fluid boundary in the soil tester was loaded by a step wave to maximum equilibrium pressure in about 1 millisecond and held constant past the time of interest. In these tests, the gauge was placed at various depths of burial close to the reflected-stress gauge where the cross section of the sample was the same as at the reflected-stress gauge.[2/] The readings from these tests in which side-wall friction was nearly zero compared favorably with readings at 1/4-inch depth in shock tube tests in which side-wall friction played a major role.

Tests were performed to evaluate the magnitude of spurious signals generated by bending of the gauge. These indicated that the polarity of the voltage output depends on the direction in which the center of the wafer was displaced. If the output during equilibrium stress in a sample contains a contribution from such a bending mode,

---

1/ This contact surface phenomenon of shock tube behavior is described in detail in Reference 5 and refers to point of separation between the quasi-steady flow regions behind the shock wave traveling into the low pressure gas and the rarefaction wave traveling into high pressure gas. Across this contact surface, the pressure and velocity are equal, but the density and temperature are generally different. The increase in pressure shown in Figure 13 is due to the reflected wave's meeting the higher density gas at the contact surface which results in an increase in pressure.

This effect has been reduced in studies on DASA Contract DA-49-146-XZ-019 by using helium as the driver gas with air as the driven gas. The lower density of the helium gas in the compression chamber relative to air at ambient pressure in the expansion chamber, helps to compensate for the normally higher density because of the higher pressure and results in a less abrupt density discontinuity at the contact surface.

2/ The effect of variations in the boundary diameter are discussed in detail in the discussion of the soil loader and sample container.

the output should be different when the gauge is turned over. To date, several such tests in 95/5 material resulted in less than 10 per cent change in equilibrium output when the gauge was turned over. In 100 per cent glass-bead material, a change of about 30 per cent was observed in the gauge of Type I design. The effect of bending is shown for Type II gauge design in Figure 15. In the reversed position the average readings at 50 psi are 7 per cent higher with a larger spread ranging from -15 per cent to +11 per cent. Since bending adds to the signal in one position and subtracts in the opposite, the error due to bending is approximately ±3.5 per cent. Variations in sample compressibility near the gauge are one source of nonuniform stress variation which could cause bending.

AIR PORE PRESSURE GAUGE

To evaluate the air pore pressure gauge, it was necessary to evaluate it for response to air pressure, to acceleration, and to intergranular stress.

To evaluate the ability of the gauge to read the pore pressure, it was necessary to make a rough calculation of the anticipated air pore pressure.

For such a rough calculation, it was assumed that the compressibility of the sample is due entirely to the reduction in the volume of the voids, hence the compression of the air under the free-field stress is related to this reduction in volume. If it is also assumed that this compression is adiabatic and that no lateral strain occurs, then the ratio of equilibrium air pore pressure to initial air pore pressure can be obtained from the relationship:

$$\frac{P}{P_o} = \left(\frac{n}{n - \frac{\Delta}{L}} \right)^r$$

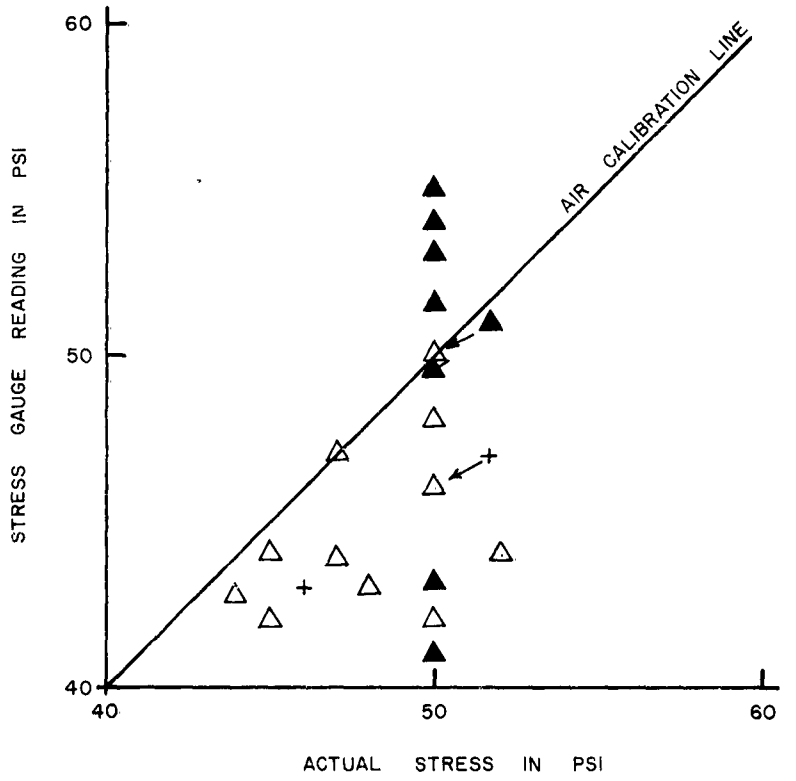

Figure 15

EFFECT OF BENDING ON FREE-FIELD STRESS GAUGE READINGS

Note: All points represent one or more data points.

Average Actual

+ △ at 1/4-inch depth in shock tube--normal position--loose Ottawa sand

▲ ▲ at 1/4-inch depth in shock tube--flipped position--loose Ottawa sand

where P = equilibrium air pore pressure

P_o = initial air pore pressure

n = initial porosity of the sample

L = initial length of the sample

Δ = change in length of the sample owing to equilibrium free-field stress

r = ratio of specific heats of air

As determined by air shock tests in the URS shock tube, the gauge has a response time to air pressure of less than 0.120 millisecond. This time is less than the rise times of the stress waves to be studies. A test of the sensitivity of the gauge to acceleration and strain effects caused by the external stress on the cup and stone was made by plugging the porous stone with glue and loading the gauge under air pressure.

The resultant output is shown in Figure 16, where it is compared with the output obtained with the same air load but with the stone unplugged. A small transient pulse was observed which was less than 0.100 millisecond in duration and had a peak value of less than 30 per cent of the applied pressure. This was followed by zero equilibrium output. The transient nature of the output indicates that the response could be due to acceleration of the cylinder.

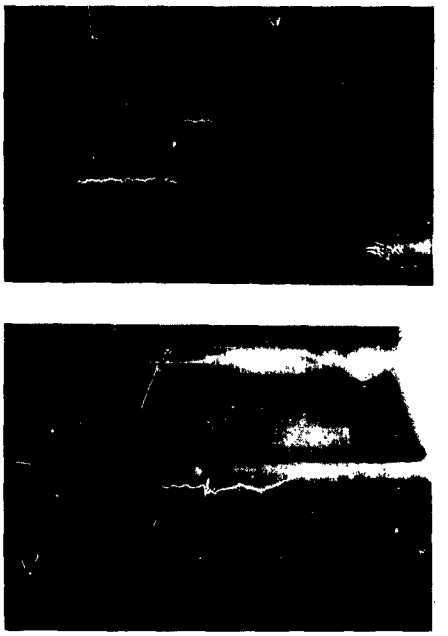

(a)

(b)

Figure 16

AIR PORE PRESSURE GAUGE OUTPUT FOR OPEN (a) AND PLUGGED (b) POROUS STONE

Note:

1/8 msec/division
3 mv/division

A typical output in response to air pore pressure during a 22-psi, 4-millisecond rise time load, in an 80/20 sample is shown in Figure 17. The equilibrium air pore pressure indicated by the gauge is approximately 8 psi. The calculated value using the Equation on page 33 for the above test is 10 psi.

SOIL LOADER AND SAMPLE CONTAINER

A number of tests were run with the complete soil loading system to check on its over-all operation, to evaluate several methods for minimizing effects of reflected pulses in the sample, and to develop procedures for obtaining uniform cross-sectional samples. Results obtained for a typical test condition are shown in Figure 18.

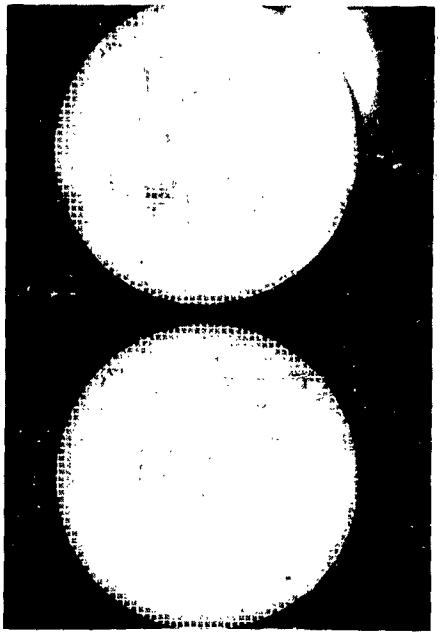

Figure 17

OUTPUT VOLTAGE VERSUS TIME OF AIR PORE PRESSURE GAUGE

Note:
1 msec/horizontal division
15 mv/vertical division

These traces were from tests in which the 20-30 Ottawa sand sample was placed at an approximate density of 103 pcf. The sample was 1-1/2 inches in diameter and 12-1/2 inches long. Separated from the air pressure by a diaphragm, the sample was loaded with an approximately square input air pressure pulse of 61 psi, 10 milliseconds long, as shown on the upper trace of Figure 18 (a). The second pulse in each of the traces was the reflected air pulse returning from the other end of the shock tube to load the sample.

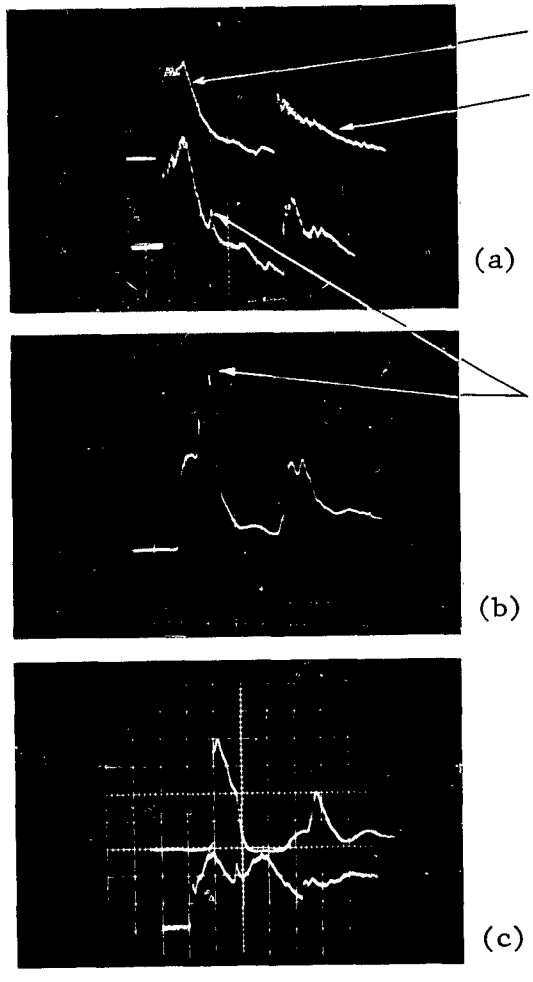

First shock tube air load

Second shock tube air load

Upper trace: Air pressure gauge--20 psi/10 v/vertical division

(a)

Lower trace: Free-field stress gauge at 1/2-inch depth--10 mv/vertical division[1/]

Reflected-stress pulse

Free-field stress gauge at 6-inch depth--10 mv/vertical division[1/]

(b)

Upper trace: Reflected-stress gauge--10 v/vertical division[1/]

Lower trace: Fluid pressure gauge--10 mv/vertical division[1/]

(c)

Figure 18

TYPICAL STRESS-WAVE TRANSMISSION RECORDS, RIGID END BOUNDARY

Note: Approximate horizontal grid scale is 2.8 msec/division.

1/ Conversion to psi requires reference to the individual calibration curve for the particular gauge because the curve does not pass through zero.

The lower trace in Figure 18 (a) shows the stress-time history 1/ at a point 1/2 inch below the air-soil boundary, with a peak reading of 55.4 psi. The trace in Figure 18 (b) shows the stress-time history at a point 6 inches below the air-soil boundary, with a peak reading before the return of the reflected-stress pulse of 54.0 psi. The upper trace in Figure 18 (c) shows the reflected stress-time history at the lower end of the soil sample at a point 12.5 inches from the air-soil boundary with a peak reading of 98 psi. The lower trace in Figure 18 (c) shows the pressure-time history of the pressure in the confining fluid, generated by the lateral stress and strain within the sample. It was measured by a gauge located in the fluid 1/2 inch below the air-soil boundary that indicated a peak reading of 15.2 psi.

The effect of the end boundary of the sample was evaluated by comparing the effect and time of arrival of the reflected stress at various stations within the sample for a rigid end boundary with those for an end boundary with mechanisms inserted at the end of the sample to delay the reflected stress. The traces shown in Figure 18, for instance, show that the reflected-stress pulse for a rigid boundary appears at the gauge locations before termination of the original pulse.

For the delay mechanisms, compressible materials were inserted at the bottom of the sample in front of the reflected-stress gauge. In one case, a piece of soft sponge rubber 1-1/2 inches in diameter and 1/2 inch thick was placed at the bottom of the soil container on top of the reflected-stress gauge, prior to placing the soil sample.

1/ The loss of the front of the pulse in this record is probably the effect of side-wall friction in the upper 3/8 inch of the sample where the sand is contained in the metal ring.

The sample was placed in the normal manner, with gauges installed at 1/2-inch and 6-inch depths below the air-soil boundary. Figure 19 presents the stress-time histories obtained in one of these tests. The unusual shape of the lower trace in Figure 19 (a), from the gauge placed at 1/2-inch depth, was due to electrical problems and was corrected in later tests. The similarity between the wave shape of the first pulse on the gauge at the 6-inch depth in Figure 19 (b) and the wave shape of the first part of the pulse, i.e. before the reflected wave arrives, on the gauge located at the same depth in the tests without the compressible material in Figure 18 (b) should be noted. A comparison of the upper trace in Figure 19 (c) with the upper trace of Figure 18 (c) will show a definite delay in the time of arrival and a distortion of the shape of the stress at the reflected-stress gauge indicating the effect of the compressible material.

An effect which will require further investigation is seen by a comparison of the lower traces in Figures 18 (c) and 19 (c) for the fluid pressure gauge. The compressible material is also sensitive to lateral loading and results in relief in lateral stress as seen in Figure 19 (c). Apparently, the fluid boundary compresses the material laterally and causes a less confined condition. This effect can be studied in the future by placing a guard ring around the compressible material to protect it from lateral stress.

A second compressible material, a 1/2-inch thick layer of diatomaceous earth, was installed in the bottom of the soil container, and the sample was prepared in the usual manner. The test results were similar to those obtained with the sponge insert.

In early tests performed in the loader using step loadings in which the equilibrium pressure was reached within 1 millisecond and maintained indefinitely, some variation in equilibrium stress readings were noted throughout the length of the sample. Generally, the stresses near the ends of the sample were the same, and those in the middle

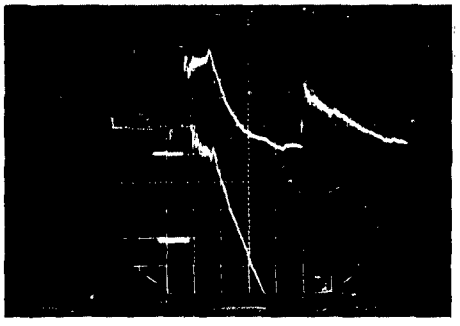

(a)

Upper trace: Air pressure gauge--20 psi/10 v/vertical division

Lower trace: Free-field stress gauge at 1/2-inch depth--10 mv/vertical division[1/]

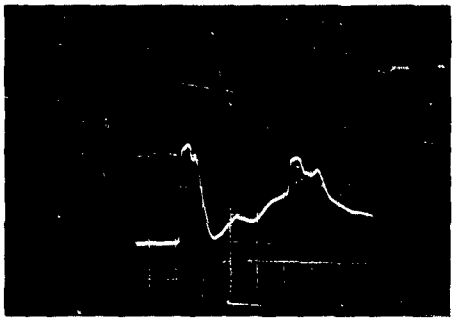

(b)

Free-field stress gauge at 6-inch depth--10 mv/vertical division[1/]

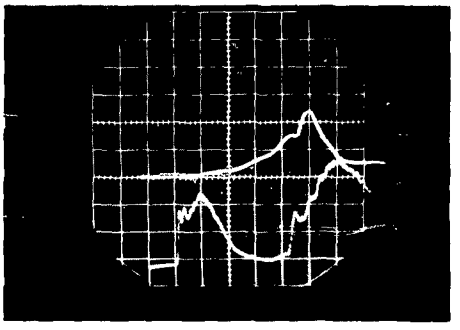

(c)

Upper trace: Reflected-stress gauge--10 v/vertical division[1/]

Lower trace: Fluid pressure gauge--10 mv/vertical division[1/]

Figure 19

TYPICAL STRESS-WAVE TRANSMISSION RECORDS, COMPRESSIBLE END BOUNDARY

Note: Approximate horizontal grid scale is 2.8 msec/division.

1/ Conversion to psi requires reference to the individual calibration curve for the particular gauge because the curve does not pass through zero.

were higher or lower. This effect was tentatively attributed to nonuniformities in the cross-sectional area of the samples.

Several tests were then performed on 1-1/2 inch long samples with nonuniform cross section, made by deliberately putting in an insufficient or excess amount of fluid in the fluid boundary. The results were qualitatively as expected; for the sample bowed out in the center, the average stress in the center cross section was less than at the ends and visa versa.

Since no simple method was available for measuring sample cross section accurately, it was concluded that the best method for getting a sample with uniform cross-sectional area was to empirically adjust the amount of fluid in the boundary until uniform stress readings were obtained throughout the length of the sample. It should be noted that the absolute magnitudes of the nonuniformities in cross section are relatively independent of sample diameter so that a larger diameter sample would make an adjustment of the amount of fluid less necessary.

OTHER EQUIPMENT

Two other pieces of equipment were evaluated to determine their possible usefulness in the work. They are the Boynton 500 psi Laboratory Dynamic Load Generator and the Filpip pressure gauge.

Boynton 500 psi Laboratory Dynamic Load Generator

To determine the planeness of the wave produced by the generator, variation in arrival time of the wave front was measured at points along a plane surface beneath the loader. Tests were made at pressures of 100, 200, and 500 psi, with pressure-time measurements being made at the center and at equally spaced points along a radius 1-13/16 inches apart. Figure 20 shows a schematic of the distribution of the front of the wave based on time of arrivals.

The results for 500 psi are tabulated below:

Distance of Gauge from Center of Loaded Plate (inches)	Arrival Time of the Wave Front[1] (microseconds)
$r_1 = 0$	$t_1 = 145$
$r_2 = 1\text{-}13/16$	$t_2 = 87$
$r_3 = 3\text{-}5/8$	$t_3 = 0$
$r_4 = 5\text{-}7/16$	$t_4 = 87$

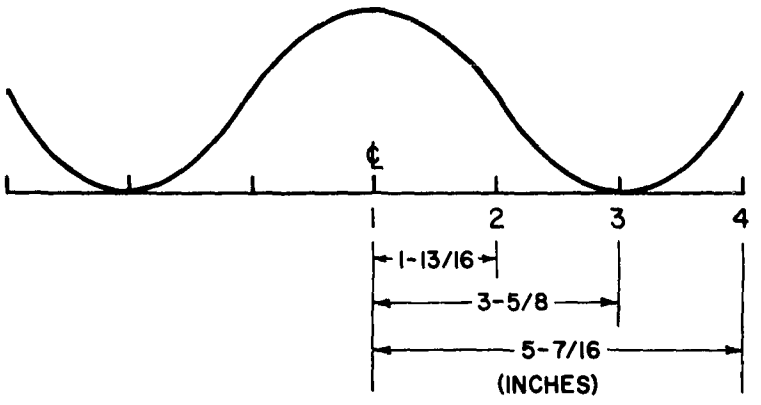

Figure 20

ASSUMED SHAPE OF THE WAVE FRONT BASED ON TIME OF ARRIVAL OF THE FRONT AT THE VARIOUS MEASURING STATIONS

1/ First arrival at any gauge is taken as t = 0, and the arrival at all other gauges are figured from that time.

A typical set of Miller oscillograph recorder traces of pressure on the various gauges versus time are shown in Figure 21.

Figure 21

PRESSURE VERSUS TIME AT VARIOUS RADII IN BOYNTON LOADER

For the other pressure levels, the wave arrived at the gauge positions in the same order as above, but with various maximum spread in time between the gauges at locations r_1 and r_3. The spread in time for these locations is given below for pressures measured:

Peak Pressure (psi)	Difference of Time of Arrival Δt (microseconds)
500	145
300	58
200	172
100	201

Filpip Pressure Transducer

In the search for a free-field stress gauge that would perform under all conditions, the Filpip capacitor type pressure transducer was suggested; one having a pressure range from 0 to 100 psi was obtained and tested. The gauge has an over-all size of 1 inch by 1 inch by 0.035 inch thick, and has a circular sensitive area 1 centimeter square. The gauge was tested in the shock tube at a depth of 1/4 inch so a comparison could be made with the air input and the data taken with the URS free-field stress gauges. The gauge output, when compared with the air calibration, read only 25 per cent of the free-field stress present. On further inquiry to the manufacturer, it was found that the gauge thickness could be compressed 0.004 to 0.006 inch under load, i.e. 11 to 17 per cent of its original thickness. As discussed in Section III and shown in Figure 12, a compressible structure such as this would be expected to have a low reading.

Section IV

STRESS-WAVE PROPAGATION TEST RESULTS

Comparison of the stress-time histories of various gauges in the stress-wave propagation tests (e.g. Figure 18) indicates that a decay of stress level with depth occurs in the 12-1/2 inch sample used. Insufficient data have been obtained to date, however, to attempt to quantitate the amount of attenuation. In addition, there still remains some uncertainty in interpretation of the reflected-stress gauge reading because a reflection factor for these conditions in soil is not known.

Based on an apparent reflection factor of 2.46 observed[1/] for the type of soil used in the work being done under DASA contract DA 49-146-XZ-019, which is the same type of soil being studied in this study, the incident stress level would be 40 psi for the 98 psi read on the reflected-stress gauge. This reflection factor would be indicative of a material having a stress-strain relationship concave about the stress axis as symbolized in Figure 22(a).

If a reflection factor of 2.00 were assumed, the incident stress level would be 49 psi. This reflection factor would be indictive of a material with a straight line stress-strain relationship symbolized in Figure 22(b). For there to be no attenuation with depth, a reflection factor of 1.77 would have to be assumed, and this would be indicative of a material having a stress-strain relationship concave about the strain axis as symbolized in Figure 22(c).

1/ The apparent reflection factors observed ranged from 2.12 to 2.46.

URS 160-12

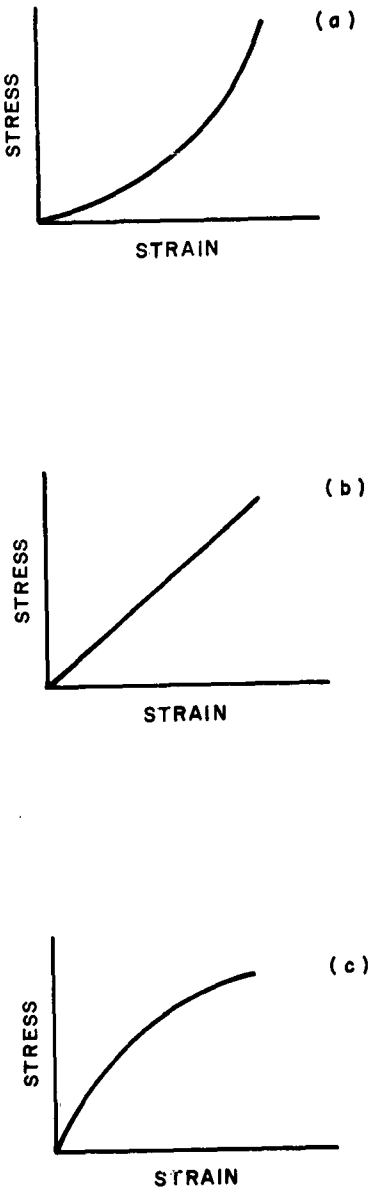

Figure 22

GENERALIZED TYPES OF STRESS-STRAIN RELATIONSHIPS OF MATERIALS EXHIBITING DIFFERENT BEHAVIOR

Data acquired under DASA contract DA 49-146-XZ-019 together with indications in the velocities obtained in this program (which will be discussed later) indicate that the stress-strain relationship for this soil under the test confinement is concave about the strain axis at lower stress levels and concave about the stress axis at higher levels. The magnitude of the stress pulse above the incident stress level caused by the reflected-stress pulse at the 6-inch depth, Figure 18 (b), was 58 psi. If it is assumed that little or no attenuation of stress occurs in the reflected pulse as it propagates back through the stressed material from the bottom to the 6-inch depth, the 58 psi can be subtracted from the 98 psi to leave 40 psi incident. This works out to give a reflection factor of 2.45 and also indicates an appreciable decay of the incident stress level with depth. Velocities of stress-wave propagation indicate that the stress-strain curve is concave about the stress axis at the upper stress levels so that the reflection factor must be greater than 2.00, again indicating an appreciable decay of stress level with depth.

A close examination of the wave shapes of the stress-time histories such as those in Figure 18 indicates some of the changes in the stress pulse that occur as a result of propagating through the soil. Since it is recognized that the changes are complex and related to stress level and stress history, related portions of the stress-time histories are compared. Comparing the slope of the initial stress rise at 1/2-inch, 6-inch, and 12-1/2 inch depths shows that the slope appears to decrease as the stress wave propagates through the soil, indicating that the lower stresses are propagating at a faster velocity than the intermediately higher stresses and that the material has a stress-strain curve with a slope concave about the strain axis in the initial portion.

The slope of the upper portion of the stress pulse appears to increase as the stress wave propagates through the soil, indicating that the upper stresses are propagating at a faster velocity than the intermediately lower stresses and that the material has a stress-strain curve with a slope concave about the stress axis at the higher stress levels.

An examination of the slope of the unloading portion of the stress pulse shows that the slope increases as the pulse moves through the soil, which is indicative of a material with a steep unloading portion on the stress-strain curve.

A crude approximation of the composite shape of the stress-strain curve for this material can be constructed from the calculated velocities listed in Table I and is shown in Figure 23.

This figure was constructed using elastic theory to compute the slope of the curve at a given stress level from the calculated velocities. In particular, starting with the amount of observed permanent strain (at 0.01in./in.) on the zero stress axis, the slope of the unloading curve was extended to the 98 psi level. At the 55 psi stress level a family of parallel lines was constructed having a slope associated with velocity of the peak stress level of the incident wave. A similar family of lines was constructed at the 25 psi stress level having a slope associated with the velocity of that level of stress of the incident wave. Next a line originating at the zero stress level was constructed at a slope associated with the velocity of the initial portion of the stress wave. A smooth curve was then drawn tangent to one line at each stress level. Next an unloading line was constructed from the 55 psi level, having a slope associated with the velocity of the peak of the unloading pulse from 55 psi (that portion of the column unaffected by the reflected-stress wave for unloading).

On the same figure is plotted an average stress-strain curve, for the same material, placed at a slightly higher density, obtained in DASA contract DA 49-146-XZ-019. In individual tests there are indications of a slight hump in the curve similar to the one constructed from the velocities that make up the average curve shown.

Table I

CALCULATED VELOCITIES IN FEET PER SECOND

	Loading Phase			Unloading Phase		Reflected-Stress Pulse
Depth[1]	Initial[2]	25 psi Level[3]	Peak[4]	Peak[5]	25 psi Level[6]	Initial[7]
1/2	340	250	550	460	940	370
6	350	360	550	980	810	710
12.5						

1/ Inches below the air-soil boundary

2/ Based on time of arrival of first indication of stress

3/ Based on time of arrival of the 25 psi level of the loading phase

4/ Based on time of arrival of the peak pressure level of the loading phase

5/ Based on time of arrival of the peak pressure level of the unloading phase (back edge of the top of the pulse)

6/ Based on time of arrival of the 25 psi level of the unloading phase

7/ Based on time of arrival of first indication of reflected stress

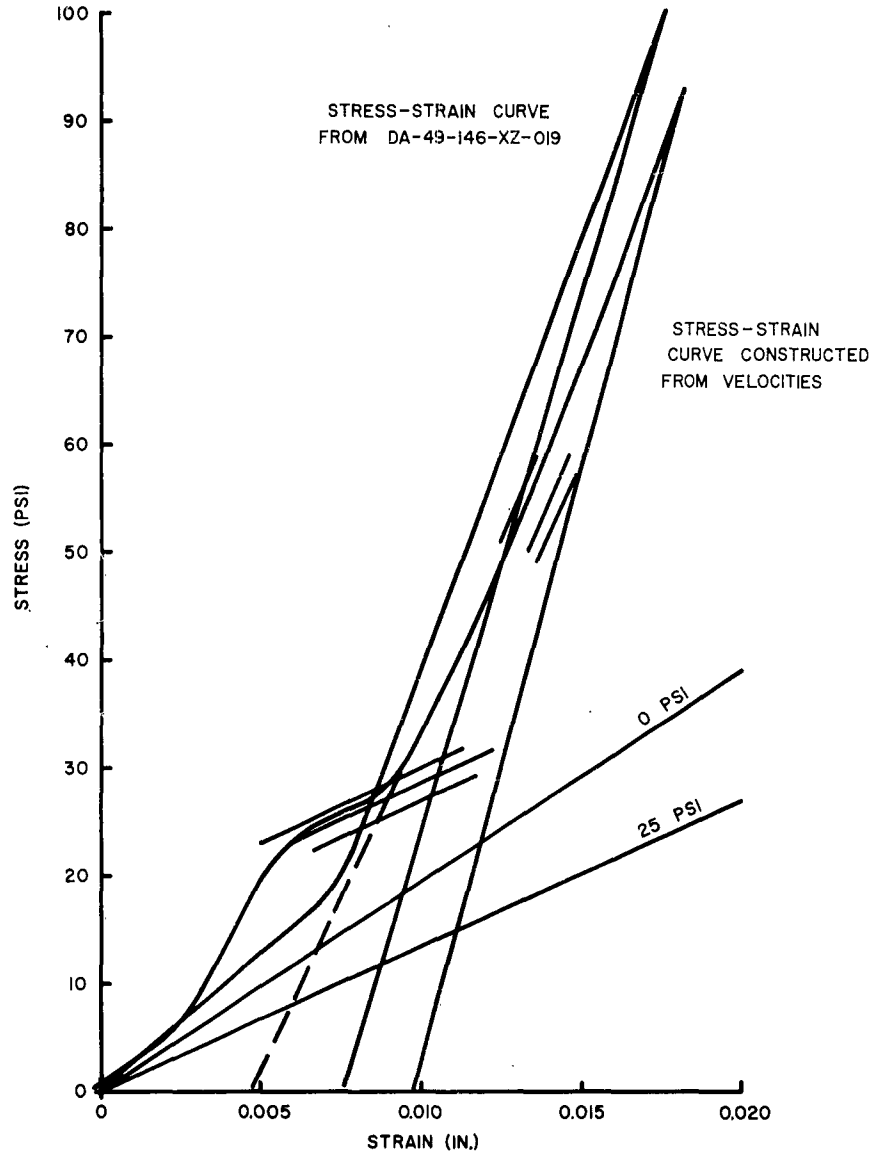

Figure 23

COMPOSITE STRESS-STRAIN RELATIONSHIP CONSTRUCTED FROM VELOCITIES

It should be emphasized that without accurate strain measurements, the construction of the stress-strain curve from velocities can be no more than conceptual in nature. However, based on the similarity between the two curves and the fact concerning the strain measurements made with the Optron Displacement Follower, the curve appears to be in the right order of magnitude.1/

Calculations of the velocities of propagations for various portions of the stress pulse for the test shown in Figure 18 were based on their times of arrival at the 1/2-inch, 6-inch, and 12-1/2 inch depths. The velocity of the leading portion of the pulse was 340 ft/sec between the 1/2-inch and 6-inch depths and 350 ft/sec between 6-inch and 12-1/2 inch depths.

A similar calculation at other stress levels is more difficult since the amount of decay as a function of depth and stress level is not know. It is possible, however, to get an idea of the velocity by comparing the time of arrivals of a particular stress level at the various depths. These velocities for the 25 psi level in the loading portion of the pulse shown in Figure 18 were 250 ft/sec in the upper depths and 360 ft/sec in the lower depths. Velocities for the peak stress value were 550 ft/sec in the upper half of the sample and 550 ft/sec for the lower half. Because of decay of stress level with depth, these numbers are probably somewhat lower than the actual velocities.

Velocities for the maximum stress level at the rear of the pulse were 460 ft/sec and 980 ft/sec in the upper and lower halves of the sample, respectively. At the 25 psi level on the unloading portion of the pulse, the velocities were 940 ft/sec for the upper half and 810 ft/sec for the lower half. The velocities for the initial portion of the reflected-stress wave were 710 ft/sec from the lower end to the 6-inch depth and 370 ft/sec from the 6-inch to 1/2-inch depths. The above velocities are tabulated in Table I.

1/ Discussed in detail on page 18.

The velocity of the initial portion of the pulse indicates that it propagates at approximately a constant velocity of 340 ft/sec until it reflects off the base. It then propagates back through the material, prestressed by the original pulse, at a much faster velocity, 710 ft/sec. After it passes through the original pulse, its velocity slows to nearly that of the original initial portion of the pulse 370 ft/sec.

Because of interference from the reflection and because of decay of the stress level with depth, calculation of the velocity of propagation of the tail is not possible with data taken to date. It is important, however, to note the rapid shortening of the total length of the pulse.

Section V

SUMMARY AND RECOMMENDATIONS

During the period from February 1960 through February 1963, URS developed soil testing apparatus and instrumentation for conducting stress-wave propagation tests.

A soil sample in which the confining pressure was generated by the lateral stress and strain in the soil and which approached the completely confined condition with a minimum of side-wall friction effect was loaded dynamically. It was shown that a controlled stress pulse could be generated of a shape that can be used to identify changes taking place in it by passing through the sample as a result of the characteristics of the soil. Observations made of velocities of stress-wave propagation tended to agree with those expected for a material with a stress-strain relationship similar to that of a confined Ottawa sand. Some initial observations concerning the effects of unloading were also made.

It was demonstrated that it is possible to affect the stress wave below the points of interest in a soil column to obtain longer periods for observation before the reflected-stress wave returns to interfere with the original pulse. Other observations indicate that it may be possible to use side-wall friction effects below the point of interest to prevent the reflected-stress wave from interfering with the original pulse. Either of these methods would permit the use of shorter samples than would otherwise be possible.

Test results indicated that the sample size used was marginal. Larger sample cross sections are needed for better control of soil and gauge placements and to reduce the variations in gauge readings resulting from small variations in cross section. A longer sample is needed so that gauges can be placed further apart to observe large changes and thereby reduce the effect of experimental error.

Certain improvements in the testing equipment are recommended. These improvements include: (1) increasing the sample diameter to 4 or 6 inches to improve control over gauge and soil placement; (2) increasing sample length to 24 inches with provisions for placing an energy absorber below the lower end; (3) continuing investigation and evaluation of the free-field stress gauge parameters to improve the accuracy, confidence level, and duration; and (4) continuing evaluation of means for measuring free-field strain or displacement, both axial and lateral.

To verify the *in situ* conditions represented by tests in the loader, it is recommended that tests be conducted in other loading configurations, such as the URS Long Duration Dynamic Loader.[1/] In addition, other conditions of confinement should be investigated.

While improvements in equipment are necessary, it is obvious that the main effort of the future work should be directed toward the detailed investigation of the influence fundamental soil and loading parameters have on stress waves propagating through the soil.

1/ See Appendix A.

LIST OF REFERENCES

1. V. W. Davis and H. G. Mason. Stress Wave Transmission Study, BRC 160-8. Burlingame, California: Broadview Research Corporation, December 1961.

2. James V. Zaccor. Techniques and Equipment for Determining Dynamic Properties of Soils, URS B155-24. Burlingame, California: United Research Services, July 1962.

3. A. H. Wiedermann. Static Experiments for the Study of the Interaction of Buried Structures with Ground Shock Waves, AFSWC-TR-61-3. Armour Research Foundation of Illinois Institute of Technology for the Air Force Special Weapons Center, April 1961.

4. A. B. Willoughby, K. Kaplan, and R. Condit. Effects of Topography on Shock Waves in Air, AFSWC-TR-57-9. Burlingame, California: Broadview Research Corporation, August 1956. Confidential.

5. I. I. Glass. Shock Tubes, Part I: Theory and Performance of Simple Shock Tubes, UTIA Review No. 12, Part I (AD 205831). University of Toronto, Institute of Aerophysics, May 1958.

Appendix A

LONG DURATION DYNAMIC LOADER

Long Duration Dynamic Loader — URS 620
United Research Services

The purpose of this company-sponsored project was to develop a loading device for dynamic and static testing on soil and soil-structure interaction problems.

The Long Duration Dynamic Loader (LDDL) was designed along principles similar to those used for the soil loaders in Projects 155 and 160,[1/] i.e. a modified shock tube principle which generates a cold gas, step pulse with an approximate rise time to maximum pressure of 1 millisecond and a continuous hold time. Similar to normal shock tube operation, the LDDL employs an inexpensive acetate diaphragm to separate the compression and expansion chambers. The soil sample is loaded with pressures up to 200 psi by bursting the acetate diaphragm. For maximum efficiency in operation, the loader is clamped by means of a hydraulic press to the soil bin which is 19 inches in diameter and 7 feet long. The LDDL has been designed to accommodate a 36-inch diameter soil bin at a later date.

1/ DASA contracts DA-49-146-XZ-019 and DA-49-146-XZ-034, respectively

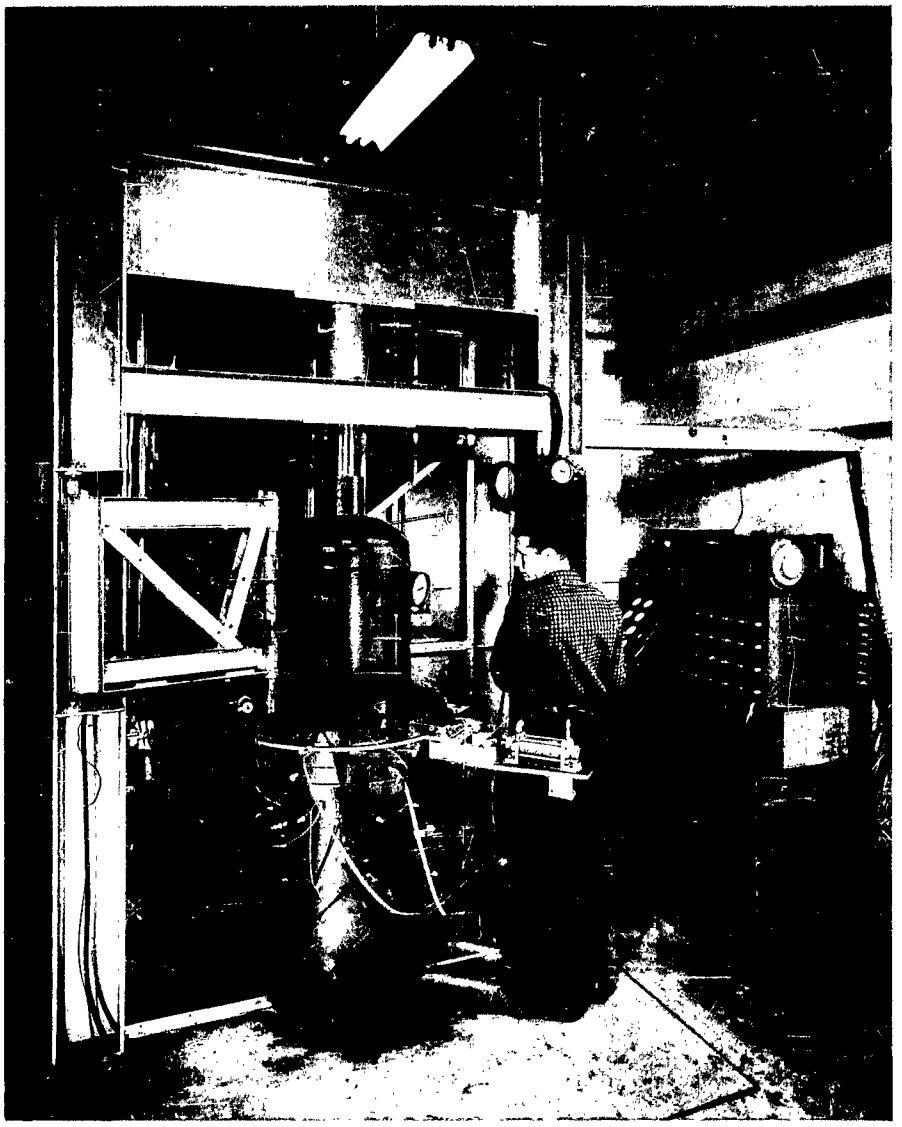

LDDL DURING TEST

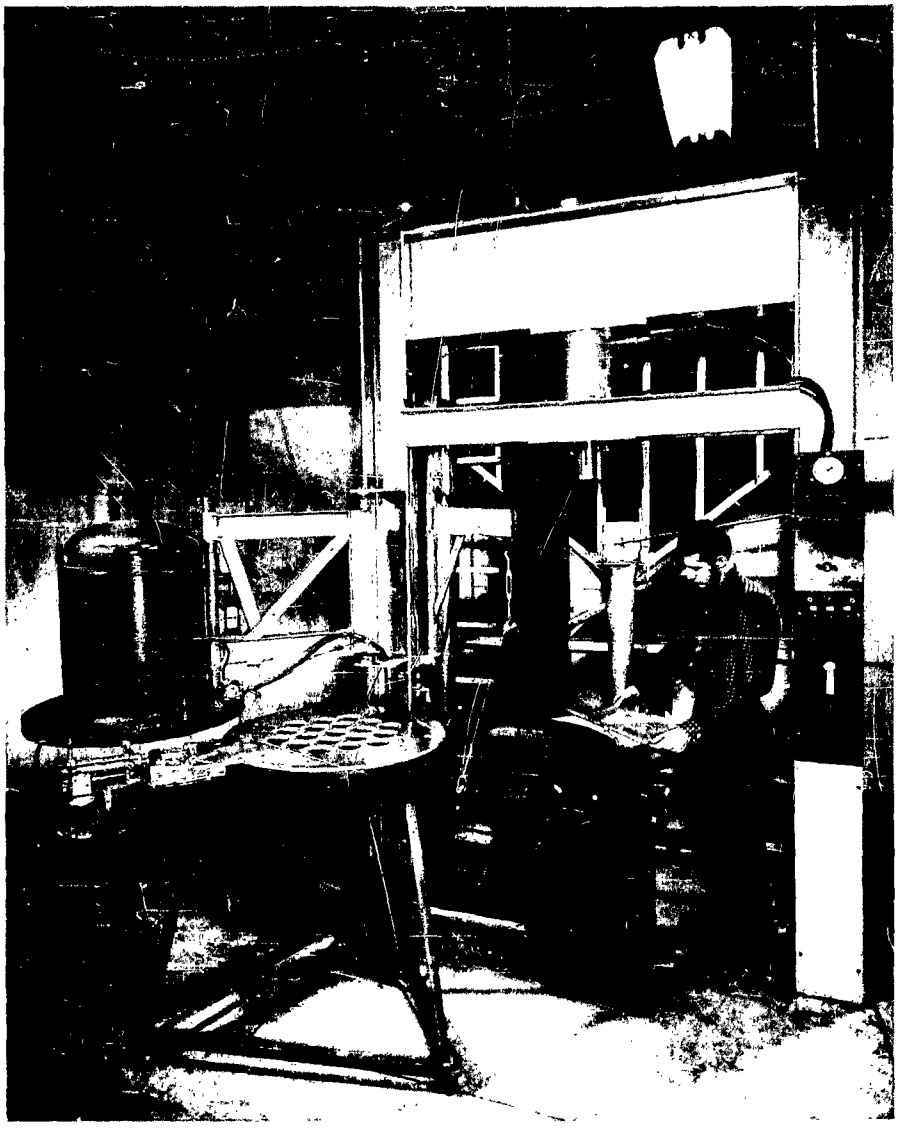

LDDL WITH COMPRESSION CHAMBER REMOVED FOR
PREPARATION OF TEST

URS 160-12

DISTRIBUTION LIST

1 Director
Waterways Experiment Station
U.S. Army Corps of Engineers
Vicksburg, Mississippi

1 Commanding Officer and Director
U.S. Naval Civil Engineering Lab.
Port Hueneme, California
Attn: Code L31

1 AFSWC (SWRS) Kirtland AFB,
New Mexico

1 Commanding General
Aberdeen Proving Ground
Aberdeen, Maryland
Attn: Director, BRL

3 Chief, Defense Atomic Support Agency
Washington 25, D.C.

1 Sandia Corporation
Sandia Base
Albuquerque, New Mexico
Attn: Classified Document Division
(for Mr. M. L. Merritt)

1 Dr. Nathan M. Newmark
University of Illinois, Room 207
Talbot Laboratory
Urbana, Illinois

1 Commander, ASTIA
Arlington Hall Station
Arlington 12, Virginia

1 Professor Robert V.
Whitman
Massachusetts Institute
of Technology, Room 1-343
Cambridge 39, Mass.

1 Dr. E. H. Chilton
Department of Physics
Stanford Research
Institute
Menlo Park, California

1 Dr. Neidhardt
General American Trans-
portation Corporation
7501 N. Natchez Ave.
Niles, Illinois

1 Paul Weidlinger
Consulting Engineer
770 Lexington Ave.
New York 21, New York
Attn: Dr. M. Baron

1 Mr. A. Weiderman
Armour Research
Foundation
10 West 35th Street
Chicago 16, Illinois